Optical Gain of Interdiffused InGaAs–GaAs and AlGaAs–GaAs Quantum Wells

K. S. Chan, *Member, IEEE*, E. Herbert Li, *Senior Member, IEEE*, and Michael C. Y. Chan

***Abstract*— We have analyzed theoretically the effects of interdiffsuion on the gain, differential gain, linewidth enhancement factor, and the injection current density of $In_{0.2}Ga_{0.8}As$–GaAs and $Al_{0.3}Ga_{0.7}As$–GaAs quantum-well (QW) lasers. We have calculated the electron and hole subband structures including the effects of valence band mixing and strains. The optical gain is then caculated using the density matrix approach. Our results show that the gain spectrum can be blue-shifted without an enormous increase in the injected current density. Imposing an upper limit (416 $A \cdot cm^{-2}$) on the injection current density for a typical laser structure, we find that the InGaAs–GaAs and AlGaAs–GaAs QW lasers can be blue-shifted by 24 and 54 nm, respectively. Our theoretical results compare well with the tuning ranges of 53 and 66 meV found for AlGaAs–GaAs QW's in some experiments. This indicates that the interdiffusion technique is useful for the tuning of laser operation wavelength for multiwavelength applications.**

***Index Terms*— Diffusion processes, quantum heterostructures, quantum-well devices, quantum-well interdiffusion, quantum-well lasers.**

I. Introduction

THE interdiffusion of III–V compound semiconductor quantum-well (QW) structures has been investigated extensively in recent years [1]–[21]. One of the reasons for the strong research interest in this technique is that it offers a simple way to modify the compositional profile of an as-grown square QW to a graded one. Apart from this, the strong dependence of interdiffusion rates on the amount of crystal defects make this technique very versatile for modifying the bandgap in a small region of a wafer by controlling the defect distribution. The interdiffusion rate can be increased by orders of magnitude in the presence of neutral or charged impurities or vacancies at group III lattice sites. If one can modify according to a pattern the compositon profile and the bandgap of a wafer, then it is not only possible to tune the operating wavelengths of optoelectronic devices for optimization but also to integrate them monolithically. It is easy to pattern the impurity distribution with a mask during ion implantation or diffusion [1]–[4], [7]–[10]. After annealing, patterns of bandgap shifts are produced. Ga vacancies, which enhance the interdiffusion rates, are usually produced by the out-diffusion of Ga atoms into a dielectric cap layer such as SiO_4 or Si_3N_4 deposited on the wafer [6], [11]–[13]. We can control the vacancy distribution and, as a result, the bandgap shifts by patterning the cap layer or depositing some diffusion barriers. This technique has the advantage of not introducing any additional impurities into the crystal.

Recently, there are a large number of experimental studies of the application of interdiffusion techniques to the fabrication of buried heterostructure lasers and the integration of lasers with different wavelengths monolithically. In the fabrication of buried heterostrucuture lasers [1]–[3], [14], [15], regions of the wafer are disordered by interdiffusion so that they become passive regions with different refractive indexes and provides optical guiding. The integration of lasers with different wavelengths is made possible by modifying the bandgaps of different regions in the wafer with interdiffsuion techniques [16]–[20]. Experimental results show that the wavelengths can be shifted significantly without a tremendous increase in the operation current of the laser. This demonstrates that interdiffusion can be used to make devices for multiwavelength applications. To understand these experimental results for the design of devices fabricated using interdifffusion techniques, it is necessary to know quantitatively how the laser characteristics are changed with the degree of interdiffusion. There is already a theoretical study by the authors [21] on the effects of interdiffusion on the gain of QW lasers, which, nevertheless, is not comprehensive in that some important characteristics such as the differential gain and linewidth enhancement factor are not included. Apart from this, the strained layer systems InGaAs–GaAs which is important for high-speed optical communication are not studied in [21]. It is the main objective of the present paper to study in detail the effects of interdiffusion on the optical gain, differential gain, and linewidth enhancement factor of AlGaAs–GaAs and InGaAs–GaAs lasers with various values of injected carrier densities. The results reported should be useful for the development of interdiffused QW lasers as they cover a wide range of operation conditions and can be used to assess the interdiffusion as a viable technique to fabricate QW lasers for multiwavelength applications.

The organization of this paper is as follows. Firstly, in Section II-A, we briefly discuss the model of interdiffusion used in the present paper and in Sections II-B and II-C we discuss the model for calculating the subband structures of the QW's and the effects of strain on the band structure in InGaAs–GaAs QW's, respectively. The formulation to determine the optical characteristics of QW lasers are presented in Section II-D. The expressions for optical matrix elements

Manuscript received March 31, 1997. This work was supported in part by the City University of Hong Kong strategic research grant, by the HKU-CRCG grant, and by the RGC Grant of Hong Kong.

K. S. Chan is with the Department of Physics and Materials Science, City University of Hong Kong, Kwoloon, Hong Kong.

E. H. Li and M. C. Y. Chan are with the Department of Electrical and Electronic Engineering, University of Hong Kong, Hong Kong.

Publisher Item Identifier S 0018-9197(98)00766-0.

TABLE I
MATERIAL PARAMETERS USED IN THE NUMERICAL CALCULATION

	$In_yGa_{1-y}As$	$Al_xGa_{1-x}As$
a (Å)	5.6533+0.405y	5.6533+0.0078x
E_g (eV)	1.425-1.501y+0.436y^2	1.424+1.594x+x(1-x)(0.127-1.31x)
C_{11} (10^{11} dyn/cm^2)	11.9-3.571y	11.9+0.12x
C_{12} (10^{11} dyn/cm^2)	5.38-0.854y	5.38-0.08x
dE_g/dP (10^{-6} eV/bar)	11.3-1.1y	11.5-1.3x
b (eV)	-1.7-0.1y	-1.7+0.2x
m_c/m_0	0.0632-0.0419y	0.0632+0.0856x+0.0231x^2
m_{hh}/m_0	0.5-0.09y	0.50+0.2x (x<0.45)
m_{lh}/m_0	0.088-0.064y	0.088+0.0372x+0.0162x^2
Δ_0 (eV)	0.34+0.07y	0.34-0.065x

are included as an appendix. In Section III, we discuss the theoretical results. We will pay particular attention to how the laser characteristics such as the gain and differential gain, etc., are affected by interdiffusion. Finally, a conclusion, which includes a comparison with experiments, is presented in Section IV.

II. THEORETICAL MODEL

A. Interdiffusion Model

Interdiffusion across the heterointerface alters the composition profile across the QW structure. In AlGaAs–GaAs and strained InGaAs–GaAs QW structures, only the interdiffusion of group-III atoms occurs, i.e., Al, In, and Ga atoms, since there is no As concentration gradient across the interface. The diffusion of group III atoms in the QW structure is usually described by the Fick's law with constant diffusion coefficients in both the well and barrier layers. The composition profile after interdiffusion is characterized by a diffusion length L_d, which is defined as $L_d = \sqrt{(Dt)}$, where D is the diffusion coefficient and t is the annealing time of thermal processing. Consider a single AlGaAs–GaAs QW with the as-grown Al mole fraction equal to x_0, the compositional profile of Al after interdiffusion is given by

$$x_{\mathrm{Al}}(z) = x_0\left\{1 - \frac{1}{2}\left[\mathrm{erf}\left(\frac{L_z + 2z}{4L_d}\right) + \mathrm{erf}\left(\frac{L_z - 2z}{4L_d}\right)\right]\right\} \tag{1}$$

where z denotes the coordinate along the crystal growth direction and L_z is the as-grown well width. The In mole fraction across the InGaAs–GaAs QW structure after interdiffusion is given by

$$y_{\mathrm{In}}(z) = \frac{y_0}{2}\left[\mathrm{erf}\left(\frac{L_z + 2z}{4L_d}\right) + \mathrm{erf}\left(\frac{L_z - 2z}{4L_d}\right)\right] \tag{2}$$

where y_0 is the as-grown In mole fraction and the QW is centered at $z = 0$.

B. Band Structure Model

To calculate the electron and hole wave functions in QW's, we use the multiband effective mass theory. For most III–V semiconductors such as GaAs-based materials, it is a good approximation that the conduction and valence bands are decoupled. A parabolic band model and the Luttinger–Kohn Hamiltonian with strain components are used for the conduction and valence bands, respectively. The electron states near the conduction subband edge are assumed to be almost purely s-like and nondegenerate (excluding spin), while the hole states near the valence subband edge are almost purely p-like and fourfold degenerate (including spin). The envelope function scheme is adopted to describe the slowly varying part of the wave function. The effects of the QW confinement potential on the energies and envelope functions of the electron and hole subband edge at the zone centre of the Brillouin zone can be calculated separately, according to the Ben–Daniel and Duke model, using the one-dimensional Schrödinger-like equation that follows:

$$-\frac{\hbar^2}{2}\frac{d}{dz}\left[\frac{1}{m^*_{\perp r}(z)}\frac{d\psi_{rl}(z)}{dz}\right] + U_r(z)\cdot\psi_{rl}(z) = E_{rl}\psi_{rl}(z) \tag{3}$$

where $\psi_{rl}(z)$ is the envelope function of the lth subband for electrons ($r = c$) or holes ($r = hh, lh$ for heavy hole and light holes, respectively), $m^*_{\perp r}(z)$ is the corresponding carrier effective mass in the z direction, E_{rl} is the subband-edge energy, and $U_r(z)$ is the confinement potential of the QW determined by considering (1), (2), and the equations for the conduction and valence band edge, which can be obtained from the material parameters given in Table I. Equation (3) is solved numerically using a finite difference method with the corresponding confinement profile.

The mixing of the light hole and heavy hole in the valence band structure, which have strong effects on the optical properties, is described by the Luttinger–Kohn Hamiltonian [22]. As a result of band-mixing, the envelope function as well as the periodic part of the Bloch wave function are functions of $k_{//}$, the wavevector in the plane perpendicular to the direction of crystal growth. To find the valence subband structures and the envelope functions of a QW, it is necessary to diagonalize the Luttinger–Kohn Hamiltonian with the appropriate confinement potentials for heavy and light holes. In this paper, we adopt the effective Hamiltonian approach described in [23] to calculate the valence subband structure. In this approach,

the hole envelope functions $\Psi_{sl}(k_{//},z)$ for spin components $s=\pm 3/2,\pm 1/2$ of the Luttinger–Kohn Hamilotonan at any finite $k_{//}$ is expressed as a linear combination of the envelope functions $\psi_{sl}(z)$ at $k_{//}=0$ as follows:

$$\Psi_s(k_{//},z)=\sum_{l=1}^{M} d_{s,l}(k_{//})\cdot\psi_{s,l}(z),\quad s=\tfrac{3}{2},-\tfrac{1}{2},\tfrac{1}{2},\tfrac{3}{2} \quad (4)$$

where $\psi_{s,l}(z)$ are the zone-center $(k_{//}=0)$ envelope functions of valence subbands obtained by solving (3) and $d_{s,l}(k_{//})$ are coefficients to be determined by the Rayleigh–Ritz variational method. $s=\pm 1/2$ and $s=\pm 3/2$ denote the light hole and the heavy hole subbands considered in (3). The accuracy of this approximation depends on M, the number of wave functions used in the linear expansion. In this study, a basis set of 40 envelope functions is used in the calculation and the results obtained are accurate within the energy range which is typical for QW laser operation. According to the Raleigh–Ritz method, the coefficients $d_{s,l}(k_{//})$ are coefficients of the eigenvectors of the following effective Hamiltonian:

$$\begin{bmatrix} \tilde{E}_{3/2}+\tilde{S}_{//} & \tilde{C} & \tilde{B} & 0 \\ \tilde{C}^{*} & \tilde{E}_{-1/2}-\tilde{S}_{//} & 0 & \tilde{B}^{T} \\ \tilde{B}^{*} & 0 & \tilde{E}_{+1/2}-\tilde{S}_{//} & \tilde{C}^{T} \\ 0 & \tilde{B}^{*} & \tilde{C}^{*} & \tilde{E}_{-3/2}+\tilde{S}_{//} \end{bmatrix} \quad (5)$$

where $\tilde{E}_s\cdot\tilde{B}$ and $\tilde{C}$ are M by M submatrices with matrix elements given by

$$C_{jj'}=\left[\frac{3}{4}\right]^{1/2}\frac{\hbar^2}{m_o}\gamma_2(k_x-ik_y)^2\int_{-\infty}^{\infty}dz\cdot\psi_{-3/2,j}(z)\,\psi_{1/2,j}(z) \quad (6a)$$

$$B_{jj'}=3^{1/2}\frac{\hbar^2}{m_o}\gamma_2(-k_x-ik_y)\int_{-\infty}^{\infty}dz\cdot\psi_{3/2,j}(z)\frac{\partial}{\partial z}\psi_{-1/2,j}(z) \quad (6b)$$

$$E_{\pm 3/2,jj'}=\delta_{jj'}E_{H,j}-\frac{\hbar^2}{2m_{//H}}k_{//}^2 \quad (6c)$$

$$E_{\pm 1,2jj'}=\delta_{jj'}E_{L,j}-\frac{\hbar^2}{2m_{//L}}k_{//}^2 \quad (6d)$$

where γ_2 is the Luttinger parameter and $j,j'=1,2,\cdots N$, $E_{H,j}$ and $E_{L,j}$ denote the jth subband energy of the heavy and light hole, respectively, and $S_{//}$ is the diagonal submatrix containing the potential due to strains in the crystal lattice, the expressions of which will be discussed in the following section.

C. Strain Effects

From the expression of the $In_xGa_{1-x}As$ lattice constant given in Table I, we can determine the strain of the interdiffused InGaAs–GaAs QW. The in-plane strain $\varepsilon(y)$ across the well depends on the In mole fraction y and therefore has the same error function profile as the composition. Assuming that the growth direction z is along $\langle 001\rangle$, then the strain components, after interdiffusion, are given by [24], [25]

$$\varepsilon_{xx}=\varepsilon_{yy}=\varepsilon(y) \quad (7a)$$

$$\varepsilon_{zz}=-2[c_{12}(y)/c_{11}(y)]\varepsilon(y) \quad (7b)$$

$$\varepsilon_{xy}=\varepsilon_{yz}=\varepsilon_{zx}=0 \quad (7c)$$

where $\varepsilon(y)$ is strain between $In_yGa_{1-y}As$ and GaAs and is defined to be negative for compressive strain, and $c_{ij}(y)$'s are the elastic stiffness constants. The change in the bulk bandgap, $S_{\perp}(y)$, due to the biaxial component of strain is given by

$$S_{\perp}(y)=-2a(y)[1-c_{12}(y)/c_{11}(y)]\,\varepsilon(y) \quad (8)$$

where $a(y)$ is the hydrostatic deformation potential calculated from

$$a(y)=-\frac{1}{3}\,[c_{11}(y)+2c_{12}(y)]\,\frac{dE_g(y)}{dP} \quad (9)$$

where dE_g/dP is the hydrostatic pressure coefficient of the lowest direct energy gap E_g. The splitting energy, $S_{//}(x_{\rm In})$, between the HH and LH band edges induced by the uniaxial strain is given by

$$S_{//}(y)=-b(y)[1+2c_{12}(y)/c_{11}(y)]\,\varepsilon(y) \quad (10)$$

where $b(y)$ is the shear deformation potential. The parameters $a,b,c_{ij},dE_g/dP$ in the above equations are assumed to obey Vegard's law and their dependence on the composition is shown in Table I. There is a coupling between the LH band and the spin-orbit split-off band due to the uniaxial strain which shifts the LH subband energies and is included using a perturbation approach as in [26]. The energy shifts of the HH and LH band edges due to the uniaxial strain are given by

$$S_{//HH}(y)=S_{//}(y) \quad (11)$$

$$S_{//LH}(y)=-1/2[S_{//}(y)+(\Delta_o(y)]+1/2[9\{S_{//}(y)\}^2\{\Delta_o(y)\}^2-2S_{//}(y)\Delta_o(y)]^{1/2} \quad (12)$$

respectively, where $\Delta_o(y)$ is the spin-orbit splitting. The QW confinement potential after the disordering process $U_r(y)$ is obtained by modifying the unstrained potential profile after processing, $(\Delta E_r(y)$, by the variable strain effects, and is given by

$$U_r(y)=\Delta E_r(y)-S_{\perp r}(y)\pm S_{//r}(y) \quad (13)$$

where $S_{\perp r}(y)=Q_rS_{\perp}(y)$, the $+$ and $-$ signs represent the confined HH and LH profiles, respectively, and $S_{//c}(y)=0$. Q_c: Q_r is the band offset ratio which is taken to be 0.7 : 0.3.

D. Gain, Differential Gain, and Linewidth Enhancement Factor

The optical gain is calculated using the density matrix approach given as

$$g(E)=\sum_{rs}\frac{2\pi q^2\hbar}{(2\pi)^2 n\varepsilon_0 c m_0^2 L_w E}\cdot\int d^2\vec{k}_{//}|\hat{e}\cdot P_{rs}(k_{//})|^2\cdot\delta(E_r^e(k_{//})-E_s^h(k_{//})-E)\times[f^e(E_r^e(k_{//}))-f^h(E_s^h(k_{//})] \quad (14)$$

where q is the electric charge, n is the refractive index, ε_0 is the dielectric constant of the vacuum, c is the speed of light, L_w is the width of the QW, E is the photon energy, P_{rs} is the optical matrix element for transition between the rth electron subband and the sth valence subband, $\hat{e}$ is a unit vector along the polarization direction of the optical electric field, and $f^e(E_r^e)$ and $f^h(E_s)$ are the Fermi distribution functions for electrons in the rth conduction and sth valence subband, respectively. Expressions for the optical matrix elements P_{rs} will be discussed in the Appendix. To include the spectral broadening of each transition, the gain in a single QW structure is convoluted with a Lorentzian line-broadening function $L(E-E')$ over all transition energies E' and is given by

$$G(E) = \int dE'\, g(E')L(E-E'). \tag{15}$$

The full width at half maximum (FWHM) of the lineshape function is about 6 meV. The expression for the spontaneous emission rate can be obtained from the gain expression by replacing the carrier occupation factor $f^e - f^h$ by the expression $f^e(1-f^h)$ and then summing over the optical modes. The differential gain dg/dN is calculated using the following expression:

$$\frac{dg}{dN}(E,N) = \lim_{\Delta N \to 0} \frac{G(E,N+\Delta N) - G(E,N)}{\Delta N} \tag{16}$$

where E is the photon energy and N is the carrier density.

The linewidth enhancement factor α is a key parameter that determines the performance of semiconductor laser both under CW operation and under high-frequency modulation. The factor α is the ratio of the change of the refractive index n with the carrier density N to the change in the optical gain g with the carrier density, which is expressed as

$$\alpha = -\frac{4\pi}{\lambda}\frac{dn/dN}{dg/dN} \tag{17}$$

where λ is the wavelength. dn/dN in (17) can be obtained from dg/dN by the Kramers–Kronig transformation.

III. Results and Discussion

In this section, we present and discuss the numerical results of lattice-matched $Al_{0.3}Ga_{0.7}As$/GaAs diffused QW's (DFQW's) and strained $In_{0.2}Ga_{0.8}As$/GaAs DFQW's. In the numerical calculation, all the room-temperature values of the material parameters are used and they are listed in Table I. Owing to the lack of space, we only consider the effects of interdiffusion on the laser characteristics of $Al_{0.3}Ga_{0.7}As$–GaAs and $In_{0.2}Ga_{0.8}As$–GaAs QW's with well widths equal to 100 Å.

A. The Subband Edge Energies and the Quasi-Fermi Energies

When the QW's are interdiffused, the potential profiles of the QW's are modified to error function profiles according to (1) and (2) given in Section II-A. The bottoms of the electron and hole confinement potentials are increased and the interband transition energies as well as the operation wavelengths are blue-shifted as a result of interdiffusion. To understand the effects of interdiffusion on characteristics such as the gain and differential gain, etc., it is necessary to know the subband energies and the subband structure. Owing to the limitation in space in the present work we only discuss the subband edge energies which have strong effects on the carrier distribution and the optical characteristics.

The subband edge energies of the interdiffused $Al_{0.3}Ga_{0.7}As$–GaAs and $In_{0.2}Ga_{0.8}As$–GaAs QW's considered here are shown in Figs. 1 and 2 as a function of L_d. It is to be noted that the zero-energy reference is taken to be the bottom of the respective QW's. We note that at the early stage of interdiffusion ($L_d < 15$ Å for both $Al_{0.3}Ga_{0.7}As$–GaAs and $In_{0.2}Ga_{0.8}As$–GaAs QW's) all the subband energies increase with the increase in L_d except for the top subband (c3 and hh3 in Fig. 1). When $L_d > 15$ Å, all the subband energies start to decrease with L_d. The increases in the subband energies are due to the reduction of the effective well widths when L_d is small. At the early stage of interdiffusion, the chemical composition at the center of the QW is changed by a negligible amount and, as a result, the potential at the center of the nonsquare QW is the same as the bottom of the square QW. So at this stage, the bottom potential of the nonsquare QW changes by a negligible amount. Since interdiffusion changes an abrupt step potential at the interface into a graded potential, the effective well widths seen by the low-lying subbands, for example, the first subband, are reduced. A detailed discussion of the effects of interdiffusion on subband structures in terms of the potential profiles in various stages of interdiffusion can be found in a previous work by the authors [27]. The highest subband bounded by the QW potential is less affected by the reduction in the effective well width as the highest subband energy is close to the barrier potential and the wave function is spread out in a wider spatial region. As a result, the highest subband energy only increases by a negligible amount when $L_d < 15$ Å.

The increases in subband energies for c2, hh2, lh1, and lh2 in $Al_{0.3}Ga_{0.7}As$–GaAs QW in Fig. 1 are larger than the increase in c1 and hh1, which leads to an increase in energy separation between the first subband and subbands lying above. In the case of $In_{0.2}Ga_{0.8}As$–GaAs QW, the increases in c2 and c3 energies are less than the increase of c1 and as a result the separation between c1 and the subbands above are reduced. For the hole subbands in the $In_{0.2}Ga_{0.8}As$–GaAs QW, the energy separations between the hh1 and hh2 are increased with L_d when L_d is less than 15 Å. We point out here that for the $In_{0.2}Ga_{0.8}As$–GaAs QW there is no bound light hole subband because the energy shift of the light hole due to the compressive strain in the InGaAs layer causes the formation of a potential barrier for the light hole in the InGaAs layer. When L_d is greater than 15 Å, the subband energies start to decrease gradually as the nonsquare QW potential starts to become shallow and the effective well width starts to increase.

The increases in the energy separations between the first subband and those lying above due to the decrease in the effective well width lead to an increase in the quasi Fermi energy (hereafter referred as Fermi energy) as more carriers can occupy the first subband. The electron and hole Fermi

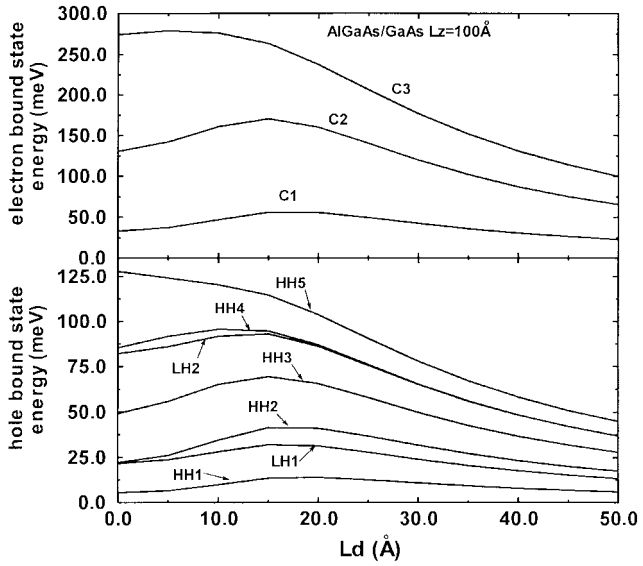

Fig. 1. The subband bound state energies as a function of L_d for interdiffused $Al_{0.3}Ga_{0.7}As$–GaAs QW with an as-grown well width of 100 Å.

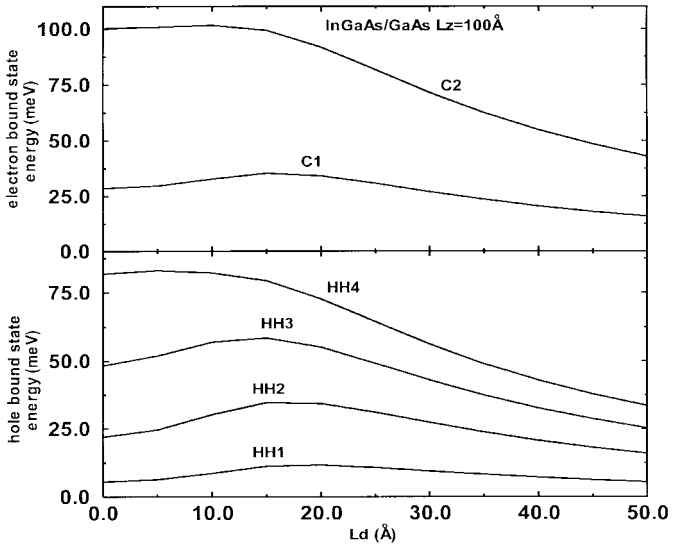

Fig. 2. The subband bound state energies as a function of L_d for interdiffused $In_{0.2}Ga_{0.8}As$–GaAs QW with an as-grown well width of 100 Å.

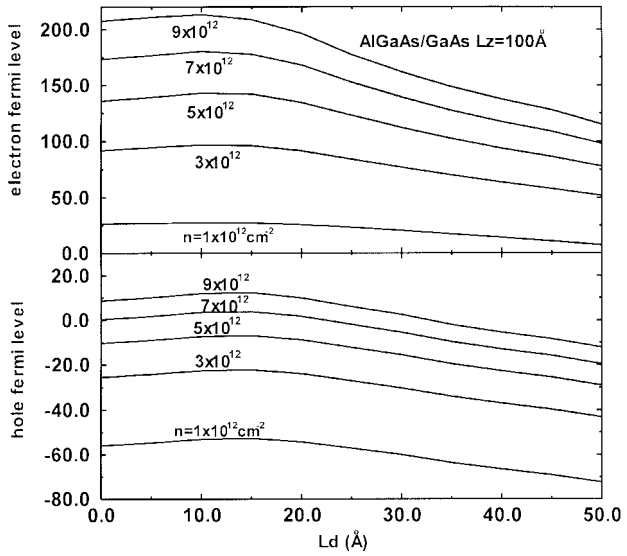

Fig. 3. The electron and hole Fermi level energies relative to the bottom of the lowest subbands plotted as a function of L_d for various injected carrier densities for the $Al_{0.3}Ga_{0.7}As$–GaAs QW.

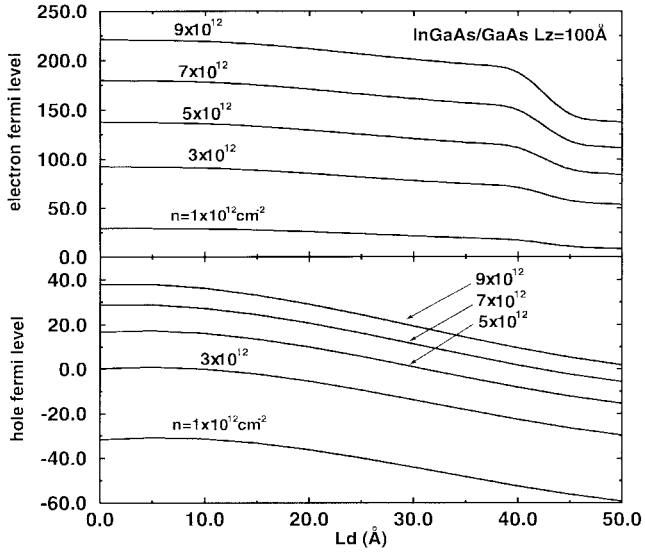

Fig. 4. The electron and hole Fermi level energies relative to the bottom of the lowest subbands plotted as a function of L_d for various injected carrier densities for the $In_{0.2}Ga_{0.8}As$–GaAs QW.

energies measured from the first subband edge are shown in Figs. 3 and 4. For $Al_{0.3}Ga_{0.7}As$–GaAs QW's, the electron and hole Fermi energies for various carrier densities shown in Fig. 3 increase slightly with L_d when $L_d < 10$ Å and then decrease for $L_d > 10$ Å. This trend can be explained by the increase in energy separations between subbands. In contrast to the $Al_{0.3}Ga_{0.7}As$–GaAs QW, the electron Fermi energy in $In_{0.2}Ga_{0.8}As$–GaAs QW starts to gradually decrease for $L_d > 0$. The gradual decrease in electron Fermi energies is the result of the reduction of energy separation between the first and second conduction subbands when L_d increases. For the hole Fermi energy, there is a negligible increase even though the separation between the first two subbands increases with L_d when $L_d < 10$ Å. The increase in the hole Fermi energy is negligible because there is an increase in the hole effective mass in the direction perpendicular to the crystal growth when the QW is interdiffused. The hole effective mass increase leads to an increase in the density of states and hence reduces the Fermi energy. The combination of the effects of the changes in energy separation and effective mass results in a negligible change in the Fermi energy. The increase in hole effective mass is due to the following two mechanisms: the outdiffusion of In atoms from the well into the barrier and the increase in valence band mixing when L_d increases. An enhancement of heavy and light hole mixing is a result of the reduction of energy separation between heavy and light hole subbands. When L_d increases, hh1, hh2, hh3, and hh4 shift upward in energy toward light hole subbands as the light hole subbands, which are above the barrier, are less affected by the changes in the potential profile. The resulting increase in subband mixing reduces the curvatures of the hole dispersion curves and increases the effective masses.

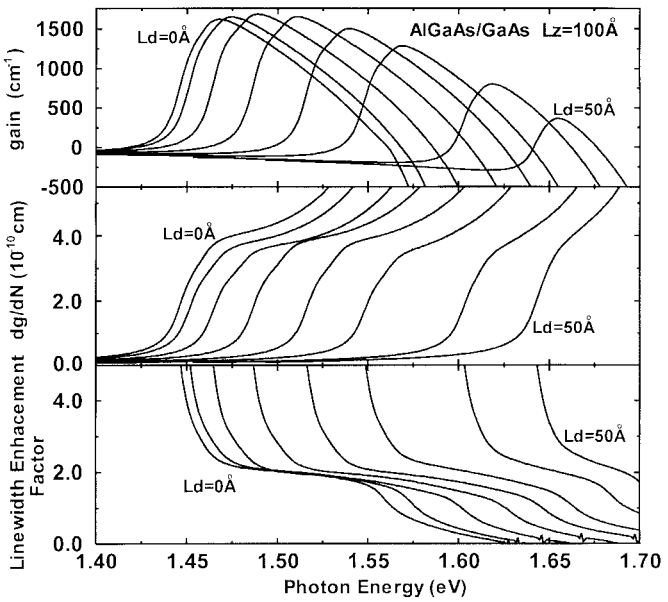

Fig. 5. The TE mode gain, differential gain, and linewidth enhancement factor of the $Al_{0.3}Ga_{0.7}As$–GaAs QW plotted as a function of photon energy for L_d = 0, 5, 10, 15, 20, 30, 40, and 50 Å.

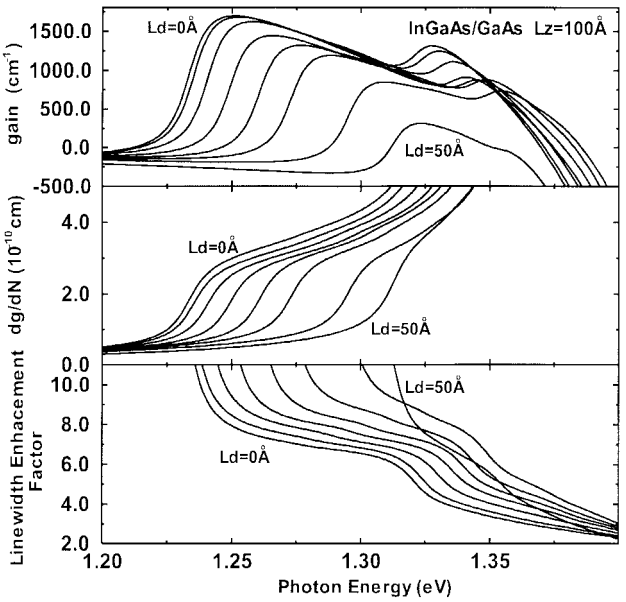

Fig. 6. The TE mode gain, differential gain, and linewidth enhancement factor of $In_{0.2}Ga_{0.8}As$–GaAs plotted as a function of photon energy for L_d = 0, 5, 10, 15, 20, 30, 40, and 50 Å.

The changes in Fermi energies discussed above will affect the optical gain through changing the conduction and valence band occupation probabilities, which will be discussed in detail in the following section.

B. Gain, Differential Gain, and Linewidth Enhancement Factor

The gain, differential gain, and linewidth enhancement factors for $Al_{0.3}Ga_{0.7}As$–GaAs and $In_{0.2}Ga_{0.8}As$–GaAs QW's are shown in Figs. 5 and 6, respectively. Only an injected carrier density of 5×10^{12} cm^{-2} is considered as the gain of the as-grown square QW with this injected density exceeds the loss (about 1200 cm^{-1}) of a typical laser structures. To calculate the loss, we take the following typical values for the optical confinement factor $\Gamma = 0.04$, laser cavity length $L = 300$ μm, and mirror reflectivity $R = 0.32$, and nonradiative absorption $\alpha = 10$ cm^{-1}. The total loss equals 48 cm^{-1} and the minimum material gain to support lasing is 1200 cm^{-1}. When the interdiffusion length (L_d) increases, the gain, differential gain, and linewidth enhancement factor spectra shift to shorter wavelengths, which is the result of the increase in transition energy between the hole and electron first subbands as the well composition changes. We notice that for the $Al_{0.3}Ga_{0.7}As$–GaAs QW the gain peak first increases by 2%–3% when L_d is increased to about 10 Å and then gradually decreases when L_d is further increased. The decrease in gain with L_d when $L_d > 20$ Å is quite rapid as the peak gain at $L_d = 20$ and 40 Å are, respectively, 95% and 50% of the peak gain of the as-grown square QW. This trend can be explained by the behavior of the Fermi energy discussed in Section III-A. The hole and electron Fermi energies for $Al_{0.3}Ga_{0.7}As$–GaAs QW's first increase when $L_d < 10$ Å and then decrease as L_d is further increased beyond 10 Å. The increases in the Fermi energies result in increases in the electron and hole occupation probabilities of the first subband and as a consequence enhance the optical gain. This increase in gain at the early stage of interdiffusion gives a range of L_d in which one can tune the operation photon energy of the laser without any deterioration of the gain and substantial increase in the injected current. Although the peak gain starts to decrease when $L_d > 10$ Å, we note that the peak gain at L_d =15 Å is approximately the same as that of $L_d = 0$. Therefore, we can shift the operation energy by about 50 meV without reducing the peak gain. A very similar trend is also observed in the numerical results for the gain of the TM mode, which is not discussed in detail here. The dependence of the gain spectra of the $In_{0.2}Ga_{0.8}As$–GaAs QW on L_d shown in Fig. 6 is markedly different from those of $Al_{0.3}Ga_{0.7}As$–GaAs in that when L_d is increased from 0 to 10 Å the gain peak of $In_{0.2}Ga_{0.8}As$–GaAs is gradually reduced in contrast with the slight increase in $Al_{0.3}Ga_{0.7}As$–GaAs. The decrease in the gain peak when increasing L_d from 5 to 10 Å is larger than the decrease due to changing L_d from 0 to 5 Å. This implies that the tuning of the laser operation wavelength with interdiffusion technique in the $In_{0.2}Ga_{0.8}As$–GaAs QW cannot be carried out without reduction in peak gain. If we want to keep the gain peak within 95% of the gain peak of the as-grown well, the operation photon energy can only be tuned by about 10 meV which is smaller than the tuning range of $Al_{0.3}Ga_{0.7}As$–GaAs. When L_d is increased beyond 40 Å, the decrease in gain is quite rapid as there is an increase in the number of conduction band bound states.

As the degree of interdiffusion increases the differential gain and the linewidth enhancement factor spectra are blue-shifted as the gain spectra. However, in contrast with the gain spectra, it is interesting to note that the differential gain and the linewidth enhancement factor around the gain peak wavelengths are not strongly dependent on L_d as the gain spectra for both AlGaAs and InGaAs QW's. In the differential

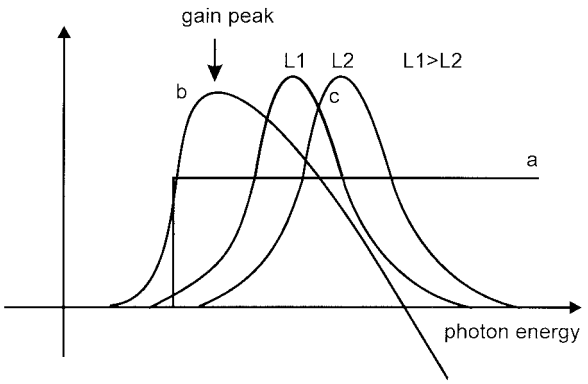

Fig. 7. The schematic diagram showing the relation between the gain spectrum, the joint density of states and the function $f^c(1-f^c)$ for $L_d = L_1, L_2$.

gain (linewidth enhancement factor) spectra, there is a shoulder (elbow) around the transition energy of the gain peak due to the step in the joint density of states near to the bandgap energy. The height of this shoulder (elbow) is approximately the largest differential gain (smallest linewidth enhancement factor) one can obtain from the material around the gain peak by tuning the operation wavelength. We notice that in both material systems the dependence of the height of the shoulder (elbow) on L_d is weak (about 10%–20%) if the carrier density is kept constant. This implies that we can tune the operation wavelength of the laser by interdiffusion without any substantial deterioration in the relaxation oscillation frequency and chirping performance. To understand the effect of interdiffusion on the differential gain [we only need to consider the differential gain here as the linewidth enhancement factor is related to the differential gain by (17)], we consider the following approximate expression of the differential gain:

$$\frac{dg}{dn} = D(E)|P|^2\left[f^c(1-f^c)\,\frac{dE_F^c}{dn} - f^h(1-f^h)\,\frac{dE_F^h}{dn}\right] \tag{18}$$

where $D(E)$ and P^2 are, respectively, the joint density of states and the optical matrix element. The term $f^c(1-f^c)\,dE_F^c/dn)$, is greater than the term $f^h(1-f^h)\,(dE_F^h/dn)$, which will be ignored in the following discussion, as the electron effective mass is smaller than the hole effective masses and dE_F^c/dn is greater than dE_F^h/dn. To illustrate the relation between the gain, $D(E)$, dg/dn, and $f^c(1-f^c)$, we show the dependence of these quantities schematically on the photon energy in Fig. 7. The function $f^c(1-f^c)$ has a peak at the Fermi energy. When L_d is increased, the electron Fermi energy is decreased so the curve for the function $f^c(1-f^c)$ shifts to the left in the schematic diagram and the value of the function $f^c(1-f^c)$ at the gain peak wavelength increases with L_d. The factor dE_F^c/dn decreases with the increase in L_d and so compensates for the increase in $f^c(1-f^c)$. As a result, the differential gain is not strongly dependent on L_d.

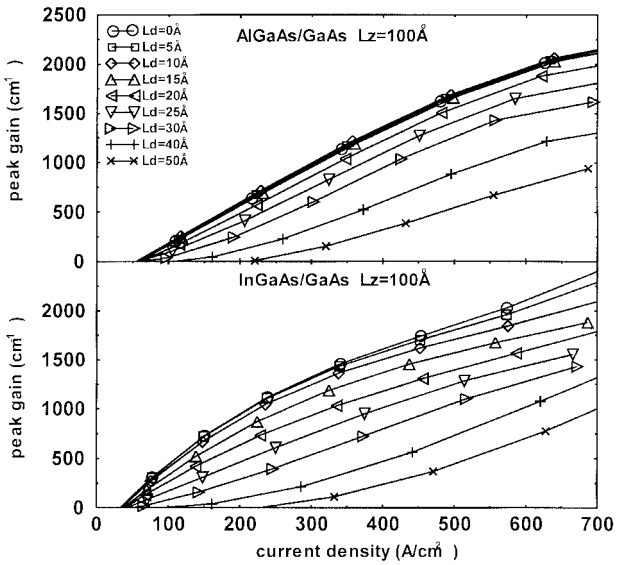

Fig. 8. The peak gain of the $Al_{0.3}Ga_{0.7}As$–GaAs and $In_{0.2}Ga_{0.8}As$–GaAs QW's plotted against the injected current density due to spontaneous emission for different L_d's. The curves for $L_d = 0$, 5, 10, and 15 Å for AlGaAs–GaAs QW are too close to be resolved.

C. Injection Current

In order to assess interdiffusion as a viable technique for shifting the operation wavelengths of lasers integrated monolithically, it is necessary to know how the injection current changes with the degree of interdiffusion. In Fig. 8, we show the dependence of the peak gain on the injected current density due to spontaneous emission for L_d between 0 and 50 Å. For $0 < L_d < 15$ Å, the peak gain of the $Al_{0.3}Ga_{0.7}As$–GaAs QW has a small dependence on L_d and thus the curves in Fig. 8 for these L_d cannot be resolved. We have ignored the components of the injection current due to other mechanisms such as carrier leakage as we are interested in the material performance in the present paper. The material peak gain shown in Fig. 8 can be compared with the loss of 1200 cm^{-1} in a typical laser structure and determine the required injected current density. From Fig. 8, the as-grown $Al_{0.3}Ga_{0.7}As$–GaAs and $In_{0.2}Ga_{0.8}As$–GaAs QW's require current densities of 320 and 220 A/cm^{-2}, respectively, to reach the lasing threshold. When L_d is increased from 0 to 50 Å, the current density should be increased to a value larger than 700 A/cm^{-2} to keep the peak gain equal to the loss, which is more than two times the current requirement of an as-grown square well. For practical operation of interdiffused QW lasers, we have to limit the injected current after interdiffusion and therefore limit the degree of interdiffusion, assuming that we can allow an increase in the injected current by 30% after interdiffusion and the peak gain is still 1200 cm^{-1}. From Fig. 8, the maximum L_d for $Al_{0.3}Ga_{0.7}As$–GaAs and $In_{0.2}Ga_{0.8}As$–GaAs QW's that still satisfy the current and gain limits are, respectively, 25 and 15 Å. The degree of interdiffusion in InGaAs QW's is smaller than that of the AlGaAs QW's, because the current density we consider for InGaAs is smaller. If we allow a current density comparable to that of AlGaAs, the L_d for InGaAs can be increased to 20 Å. We have also plotted the peak wavelength of the

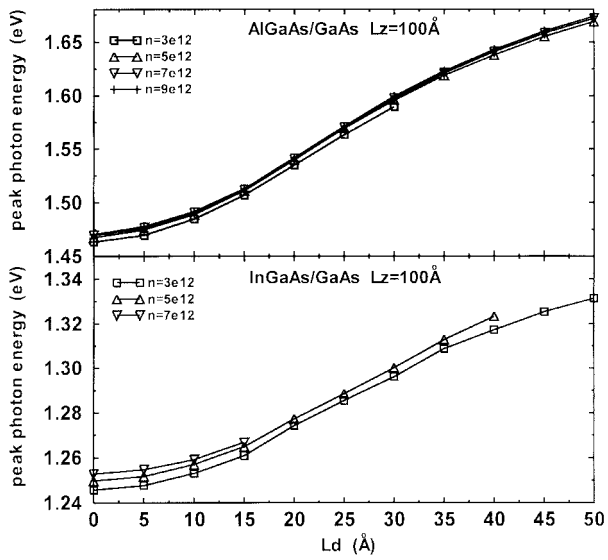

Fig. 9. The photon energy of the peak of the gain spectrum plotted as a function of L_d for different carrier densities.

gain spectrum versus L_d for various well carrier densities in Fig. 9 in order to determine the tuning capability of the interdiffusion technique. We notice that the peak wavelengths of the laser gain spectrum for $Al_{0.3}Ga_{0.7}As$–GaAs is quite insensitive to the carrier density but is strongly dependent on the value of L_d. For $In_{0.2}Ga_{0.8}As$–GaAs QW's there is a strong dependence of the peak wavelengths on L_d and a noticeable dependence on the carrier density. In the present case, we find from Fig. 9 that the $Al_{0.3}Ga_{0.7}As$–GaAs QW can be tuned by about 100 meV, equivalent to 54 nm. The tuning range for $In_{0.2}Ga_{0.8}As$–GaAs is about 15 meV, which equals 12 nm. The tuning range of $In_{0.2}Ga_{0.8}As$–GaAs is limited as we restrict the current density between 220 and 286 A/cm^{-2}. Nevertheless, if we allow the current density to increase to the limit for the $Al_{0.3}Ga_{0.7}As$–GaAs QW (416 A/cm^{-2}), the wavelength tuning range is increased to 24 nm corresponding to a change in photon energy of about 30 meV.

IV. Conclusion

We have analyzed theoretically the effect of interdiffusion on the laser characteristics of $Al_{0.3}Ga_{0.7}As$–GaAs and $In_{0.2}Ga_{0.8}As$–GaAs QW's. We have modeled the composition profile of interdiffused QW's using error function profiles and calculated the subband structures including the effects of valence band mixing using an effective Hamiltonian approach. The optical gain, the differential gain, and linewidth enhancement factors can be calculated from the subband structures using the density matrix approach and the Kramers-Kronig transformation. Our results show that the operation wavelength can be blue shifted by the interdiffusion techniques without any impractical increase in the injected current density. The peak gain of AlGaAs QW's is increased by less than 10% by interdiffusion when L_d is less than 15 Å and drops below the peak gain of the as-grown square well when $L_d > 15$ Å. For InGaAs QW's, the peak gain begins to decrease when $L_d > 0$. These behaviors can be explained in terms of the effects of interdiffusion on the electron and hole quasi-Fermi energies. As a result, the tuning range (10 meV) of InGaAs QW's is smaller than that of the AlGaAs QW's (50 meV) for a fixed injected carrier density and an allowed variation of peak gain within 10% of the as-grown value. In practice, we can increase the tuning range by increasing the injected carrier density in the application of the technique to laser fabrication. To study this aspect, we have calculated the peak gain as a function of the injected current density as well as the interdiffusion length L_d. For a maximum injection current density of about 416 A/cm^{-2}, the tuning range of AlGaAs and InGaAs QW's are, respectively, 54 and 24 nm, which is acceptable for multiwavelength applications. The tuning range can also be increased by allowing a higher injection current density.

It is interesting to compare our results with some experiments. Meehan *et al.* [16] have obtained an emission energy tuning range of 53 meV by interdiffusion for a double QW laser at 300 K. The injected current is increased from 555 to 675 A/cm^{-2} after the laser is interdiffused. Since there are two QW's, the current required for each QW is approximately 277 and 338 A/cm^{-2} for the as-grown and interdiffused QW's, respectively. Nagai *et al.* [20] have obtained a shift in energy of 66 meV while the threshold current increases by about 33% for a 60 Å AlGaAs–GaAs QW. Although some details of the devices studied in these experiments are not known, we can still make some approximate comparisons. From Figs. 8 and 9, we find that when the current is increased from 270 to 338 A/cm^{-2}, the corresponding increase of L_d is from 0 to about 20 Å and the gain peak energy is shifted by about 55 meV. This theoretical tuning range is close to those found in experiment. As a conclusion, our study shows that the interdiffusion technique is useful for tuning the operation wavelengths of QW lasers for communication applications.

Appendix
Optical Matrix Element

When the subband envelop functions are obtained, the optical matrix elements can be calculated by the following expression:

$$P_{rs} = \langle r|\vec{p}|s\rangle \tag{A1}$$

where r and s denote the Bloch functions of electron or holes and $|r\rangle = \psi(z)|u\rangle e^{i\vec{k}\cdot\vec{r}}$, $\psi(z)$ is the envelope function along the z direction, and $|u\rangle$ is the periodic and rapidly varying part of the Bloch function. The periodic part of the Bloch function for electrons (hereafter referred as the Bloch states) are given by

$$\begin{aligned} |u^e_{1/2}\rangle &= |s\rangle \uparrow \\ |u^e_{-1/2}\rangle &= |s\rangle \downarrow \end{aligned} \tag{A2}$$

where $\uparrow$ and $\downarrow$ denote the up and down electron spinors and $|s\rangle$ is the s-like conduction-band Bloch state. For holes, the Bloch states are represented by the linear combinations of the

products of the spinor and the p-like valence-band Bloch states $|p_s\rangle, |p_y\rangle$, and $|p_z\rangle$ are given by

$$\begin{aligned}
|u^h_{3/2}\rangle &= \frac{-1}{\sqrt{2}}\,(|p_x\rangle + i|p_y\rangle)\uparrow \\
|u^h_{1/2}\rangle &= \frac{-1}{6}\,[(|p_x\rangle + i|p_y\rangle)\downarrow -2|p_z\rangle\uparrow] \\
|u^h_{-1/2}\rangle &= \frac{1}{6}\,[(|p_x\rangle - i|p_y\rangle)\uparrow +2|p_z\rangle\downarrow] \\
|u^h_{-3/2}\rangle &= \frac{1}{\sqrt{2}}\,(|p_x\rangle - i|p_y\rangle)\downarrow . \qquad \text{(A3)}
\end{aligned}$$

The squared of optical matrix elements for the TE polarization (the optical electric field is polarized in the x–y plane) and the TM polarization (the optical electric field is polarized in the z direction) are obtained within the envelope function approximation.

(1) For the TE polarization,

$$\begin{aligned}
|\hat{e}\cdot P_{pq}(k_{//})|^2 = &|\langle x|p|s\rangle|^2 \\
&\cdot [\tfrac{1}{2}\,(|\langle\psi^e_p|\psi_{3/2,q}\rangle|^2 + |\langle\psi^e_p|\psi_{-3/2,q}\rangle|^2) \\
&+ \tfrac{1}{6}\,(|\langle\psi^e_p|\psi_{-1/2,q}\rangle|^2 + |\langle\psi^e_p|\psi_{1,2,q}\rangle|^2)] \qquad \text{(A4)}
\end{aligned}$$

(2) For the TM polarization,

$$\begin{aligned}
|\hat{e}\cdot P_{pq}(k_{//})|^2 = &\tfrac{3}{2}\,|\langle x|p|s\rangle|^2 \\
&\cdot (|\langle\psi^e_p|\psi_{-1/2,q}\rangle|^2 + |\langle\psi^e_p|\psi_{1/2,q}\rangle|^2) \qquad \text{(A5)}
\end{aligned}$$

where $\langle\psi^e_p|\psi_{s,q}\rangle$ is the overlap integral of the envelope functions. The expression for $\langle x|P_x|s\rangle$ is

$$|\langle x|P_x|s\rangle|^2 = \frac{m_0^2}{2m_e}\,\frac{E_g(E_g+\Delta)}{E_g+\frac{2}{3}\,\Delta} \qquad \text{(A6)}$$

where Δ is the spin-orbit splitting energy, E_g is the bandgap energy, and m_e is the electron effective mass. The expressions of $\psi_{s,q}$ $(s=-3/2,\cdots,3/2)$ are given by (4).

REFERENCES

[1] T. Fukuzawa, S. Semura, H. Saito, T. Ohta, Y. Uchida, and H. Nakashima, "GaAlAs buried multiquantum well lasers fabricated by diffusion-induced disordering," *Appl. Phys. Lett.*, vol. 45, pp. 1–3, 1984.

[2] P. Gavrilovic, K. Meehan, L. J. Guido, N. Holonyak, Jr., V. Eu, M. Feng, and R. D. Burnham, "Si-implanted and disordered strip-geometry $Al_xGa_{1-x}As$-GaAs quantum well lasers," *Appl. Phys. Lett.*, vol. 47, pp. 903–905, 1985.

[3] D. F. Welch, D. R. Scifres, P. S. Cross, and W. Streifer, "Buried heterostructure lasers by silicon implanted, impurity induced disordering," *Appl. Phys. Lett.*, vol. 51, pp. 1401–1403, 1987.

[4] J. Werner, E. Kapon, N. G. Stoffel, E. Colas, S. A. Schwarz, C. L. Schwartz, and N. Andreadakis "Integrated external cavity GaAs/AlGaAs lasers using selective quantum well disordering," *Appl. Phys. Lett.*, vol. 55, pp. 540–542, 1989.

[5] I. Harrison, H. P. Ho, and N. Baba-Ali, "Diffusion induced disorder of GaAs/AlGaAs Superlattice," *J. Electron. Mater.*, vol. 20, pp. 449–456, 1991.

[6] A. Wakatsuki, H. Iwamura, Y. Suzuki, T. Miyazaawa, and O. Mikami, "Refractive index change of GaInAs/InP disordered superlattice waveguide," *IEEE Photon. Technol. Lett.*, vol. 3, pp. 905–907, 1991.

[7] J. Z. Wan, D. A. Thompson, and J. G. Simmons, "Ion implantation induced compositional intermixing in the InGaAs/InP MQW system for wavelength shifted waveguides," *Nuclear Inst. Meth. Phys. Res. B*, vol. 106, pp. 461–465, 1995.

[8] K. B. Kahen and G. Rajeswaran, "Study of the interdiffusion of GaAs-AlGaAs interfaces during rapid thermal annealing of ion-implanted structures," *J. Appl. Phys.*, vol. 66, pp. 545–551, 1989.

[9] K. B. Kahen, G. Rajeswaran, and S. T. Lee, "Mechanism for ion-induced mixing of GaAs-AlGaAs interfaces by rapid thermal annealing," *Appl. Phys. Lett.*, vol. 24, pp. 1635–1637, 1988.

[10] W. D. Laidig, N. Holonyak, Jr., M. D. Camras, K. Hess, J. J. Coleman, P. D. Dapkus, and J. Bardeen, "Disorder of an AlAs-GaAs superlattice by impurity diffusion," *Appl. Phys. Lett.*, vol. 38, pp. 776–778, 1981.

[11] K. B. Kahen, D. L. Peterson, G. Rajeswaran, and D. J. Lawrence, "Properties of Ga vacancies in AlGaAs materials," *Appl. Phys. Lett.*, vol. 55, pp. 651–653, 1989.

[12] T. Miyazawa, H. Iwamura, and M. Naganuma, "Integrated external-cavity InGaAs/InP lasers using cap-annealing disordering," *IEEE Photon. Technol. Lett.*, vol. 3, pp. 421–423, 1991.

[13] H. Ribot, K. W. Lee, R. J. Simes, R. H. Yan, and L. A. Coldren, "Disordering of GaAs/AlGaAs multiple quantum well structures by thermal annealing for monolithic integration of laser and phase modulator," *Appl. Phys. Lett.*, vol. 55, pp. 672–674, 1989.

[14] K. Meehan, P. Gavrilovic, and N. Holonyak, Jr., R. D. Burnham, and R. L. Thornton, "Stripe-geometry $Al_xGa_{1-x}As$-GaAs quantum well heterostructure lasers defined by Si diffusion and disordering," *Appl. Phys. Lett.*, vol. 46, pp. 75–77, 1985.

[15] P. Gavrilovic, K. Meehan, J. E. Epler, and N. Holonyak, Jr., "Impurity-disordered, coupled-stripe $Al_xGa_{1-x}As$/GaAs quantum well laser," *Appl. Phys. Lett.*, vol. 46, pp. 857–859, 1985.

[16] K. Meehan, J. M. Brown, P. Gavrilovic, N. Holonyak, Jr., R. D. Burnham, T. L. Paoli, and W. Streifer, "Thermal-anneal wavelength modification of multiple-well p-n $Al_xGa_{1-x}As$-GaAs quantum-well lasers," *J. Appl. Phys.*, vol. 55, pp. 2672–2675, 1984.

[17] M. D. Camras, N. Holonyak, Jr., R. D. Burnham, W. Streifer, D. R. Scifres, T. L. Paoli, and C. Lindstrom, "Wavelength modification of AlxGa1-xAs qunatum well heterostructure lasers by layer interdiffusion," *J. Appl. Phys.*, vol. 54, pp. 5637–5641, 1983.

[18] S. O'Brien, J. R. Shealy, F. A. Chambers, and G. Devane, "Tunable (Al)GaAs lasers using impurity-free partial interdiffusion," *J. Appl. Phys.*, vol. 71, pp. 1067–1069, 1992.

[19] P. J. Poole, S. Charbonneau, M. Dion, G. C. Aers, M. Buchanan, R. D. Goldberg, and I. V. Mitchell, "Demonstration of an ion-implanted wavelength-shifted quantum well lasers," *IEEE Photon. Technol. Lett.*, vol. 8, pp. 16–18, 1996.

[20] Y. Nagai, K. Shigihara, W. Karkida, S. Kakimoto, M. Otsubo, and K. Ikeda, "Characteristics of laser diodes with a partially intermixed GaAs-AlGaAs quantum well," vol. 31, pp. 1364–1370, 1995.

[21] E. H. Li and K. S. Chan, "Laser gain and current density in a disordered AlGaAs/GaAs quantum well," *Electron. Lett.*, vol. 29, pp. 1233–1234, 1993.

[22] J. M. Luttinger and W. Kohn, "Motion of electrons and holes in perturbed periodic fields," *Phys. Rev.*, vol. 97, pp. 869–883, 1955.

[23] K. S. Chan, "The effects of the hole subband mixing on the energies and oscillator strengths of excitons in a quantum well," *J. Phys. C: Solid State Phys.*, vol. 19, pp. 125–130, 1986.

[24] D. Ahn and S. L. Chuang, "Optical gain in a strained quantum-well laser," *IEEE J. Quantum Electron.*, vol. 24, pp. 2400–2406, 1988.

[25] S. L. Chuang, "Efficient band-structure calculations of strained quantum wells," *Phys. Rev. B*, vol. 43, pp. 9649–9661, 1991.

[26] R. People, "Indirect bandgap of coherently strained Ge_xSi_{1-x} bulk alloys on $\langle 001\rangle$ silicon substrates," *Phys. Rev. B*, vol. 32, pp. 1405–1408, 1985.

[27] E. H. Li, B. L. Weiss, and K. S. Chan, "Effects of interdiffusion on the subbands in an $Al_xGa_{1-x}As$/GaAs single-quantum-well structure," *Phys. Rev. B*, vol. 46, pp. 15181–15192.

K. S. Chan (M'88), photograph and biography not available at the time of publication.

E. Herbert Li (S'87–M'88–SM'95), for biography, see this issue, pp. 92.

Michael. C. Y. Chan, photograph and biography not available at the time of publication.